# A Contact Stress Capacity Model for Cylindrical Wormsets

**Edward E. Osakue**
Department of Industrial Technology
Texas Southern University
Houston, Texas,
USA

**Lucky Anetor**
Department of Engineering
Texas Southern University
Houston, Texas,
USA

*A contact stress capacity expression is derived for cylindrical worm sets by considering the worm as a helical rack mating with a helical gear. The concept of the equivalent spur gear for a helical gear defined by the instantaneous radius of curvature in the virtual plane of the helical gear is utilized in the contact stress capacity model formulation. All the basic design parameters of worm and gear are incorporated in the expression which explicitly shows the influence of the base and nominal helix angles on the contact stress. By considering the geometry of the worm and gear in engagement, active gear face width and active threaded length of the worm are defined and used to estimate load sharing among gear teeth. This allows the interaction of motion and forces in wormset meshes to be captured by a semi-empirical factor, an aspect not previously considered. The new model also accounts for multiple threaded worms which seem not to have been treated till now. The service load factor expression for cylindrical gears is modified for wormsets to take account of different worm thread profile designs and mesh friction.*

*Four illustrative examples of contact stress computations are carried out using the new contact stress capacity model for wormset designs from different references. The contact stress estimates from the new model are compared with previous solution values. The estimated percentage variances between the previous and new model values are within the range of -4.5% to 0.3%. These variances indicate excellent to a very favorable comparison that should inspire some confidence in using the new model for preliminary design tasks of cylindrical wormsets.*

*Keywords: Worm gears, Contact stress, Pitting, Helix angle, Effective lengths*

## 1. INTRODUCTION

A worm gear drive consists of a worm and gear and is also called a wormset. The worm and gear in a wormset are mounted on shafts that are non-parallel and non-intersecting that are often at right angles to each other. There are two common types of worm gear sets which are cylindrical and globoid. Fig. 1a shows a diagram of a cylindrical wormset, while Fig. 1b shows that of a globoid wormset, [1-3].

A cylindrical wormset is a single-enveloping or single-throated wormset that consists of a cylindrical worm with straight edges engaging a throated gear that partly wraps around the worm. The wrapping provided by throating helps to improve the contact between the worm and gear. A globoid wormset is a double-enveloping or double-throated wormset that consists of a throated worm with curved sides engaging a throated gear. Cylindrical worms are more popular than globoid wormsets due to manufacturing difficulties associated with globoid drives, but they have higher power capacity for the same size as cylindrical drives. Further discussions are limited to cylindrical wormsets, though the principles outlined may equally apply to globoid wormsets.
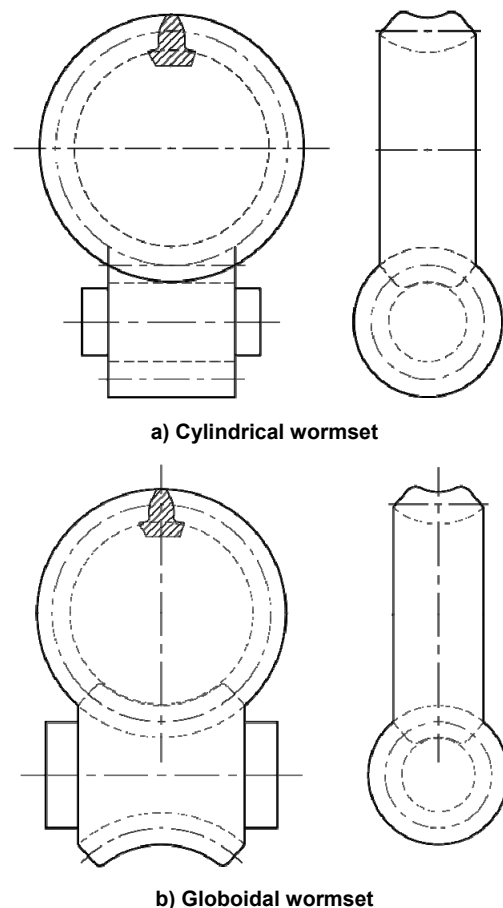
**a) Cylindrical wormset**



**b) Globoidal wormset**

**Fig. 1: Types of worm gearsets.**

Worm drives give a high transmission ratio, are of small size, have low weight, and are compact in construction. The usual range of speed ratio is from 5 to 100, but special units with a speed ratio of 360 – 400 and above are possible. In motion transmission devices (e.g., instruments) speed ratio of 1000 is possible. Due to the action of the worm, wormsets are quiet in operation, largely free of vibration, and give a constant output speed that is free of pulsations [4]. They are the smoothest and most quiet form of gear drives [5]. A major disadvantage of worm drives is their relatively large slip velocity in the mesh during operations. This causes higher frictional losses, thereby lowering transmission efficiency.

A worm may be considered as a helical rack, but it is practically a special type of power screw. The thread profile of a worm may be trapezoidal, involute, or some other profile [1]. The common worm thread profiles are designated as ZA, ZN, ZK, and ZI [2]. The ZA has a trapezoidal section with straight sides in the axial plane while the ZN has a trapezoidal section with straight sides in the normal plane. The ZK has a convex profile in the normal plane and concaves in the axial section. The ZI has an involute profile in the transverse section like a helical gear. A special worm with a concave profile in the axial section is CAVEX. It offers better contact conditions and higher load capacity. In common practice, straight cylindrical worms with a trapezoidal profile of 40° included angle and gear of involute profile are used in wormsets [1, 2]. The axial pitch of the worm screw is equal to the circular pitch of the gear. Note that the radial section of the worm corresponds to the axial section of the gear and verse versa. However, the pair shares a common normal section, which is often used for defining wormset profiles by specifying the normal module as a standard module. The advantage of this is that ordinary gear hobs can be used to cut the gear.

The preferred pressure angle for worms with a lead angle less than 30° is 20°. A pressure angle of 25° is used for the lead angle between 25° and 35° and the pressure angle of 30° is used for the lead angle between 35° and 45° [6]. Generally, higher lead angles give higher efficiencies, however, the lead angle is usually restricted to 45° but can be as high as 50° practically [7]. It is relatively more difficult to manufacture worms with a lead angle of more than 25⁰ [8]. The hand and helix angle of the gear is the same as the hand and lead angle of the worm, respectively. The meshing action in wormsets is similar to that of helical gears except that the sliding velocity is much higher [6]. The engagement of a throated helical gear and a worm is analogous to a nut mating with a screw [9, 10].

Generally, worm gear failure may result from pitting, abrasive wear, scuffing, or breakage, like other types of gears. However, properly sized, and run-in wormsets that are not overloaded or overheated can give a very long service life and may ultimately fail by pitting in surface fatigue [9]. But the high sliding velocity makes scuffing a highly probable failure mode compared to the other types of gears [11]. The risk of seizure is associated with scuffing that is dependent on the contact stress and the degree of overheating. To minimize failure by scuffing, the contact stress is reduced compared to cylindrical gears. A hunting tooth on the gear helps to distribute wear more evenly amongst gear teeth. Gear tooth failure due to bending fracture is rare in worm gearsets [9] if well-designed. Breakage is more likely with gears having a large number of teeth say over 100 or fine-module gears [1]. Bending failure could be seriously damaging and should be avoided.

Worm profiles are more complex than involute tooth profiles [12]. Therefore, the recommended design approach for wormsets by many gear standards is largely empirical. Though some attempts have been made by various researchers and organizations to develop a power rating system for worm gears, it appears this has been somewhat elusive. The problem is that the long-term success of worm drives depends on many factors that are more difficult to adequately quantify compared to other types of gears [12].

The objective of this study is to develop a more scientific and rational approach to the estimation of contact stress of cylindrical wormsets. Contact mechanics and geometric principles are combined with experimental data in the formulation of a new contact stress capacity expression. Because practical design is strongly tied to experience and experimentation, empirical factors can hardly ever be eliminated in engineering model capacity formulations, however, they can be minimized. The approach presented is systematic and has only one semi-empirical factor for worm contact effectiveness in load sharing and one empirical factor for worm type profiles added to those factors commonly used in cylindrical gears.

## 2. WORMSET BASIC KINEMATICS

The geometry of a worm is similar to that of a power screw and its rotation simulates a linearly advancing rack. The lead is equal to the axial distance traveled by a point on the worm-screw in one revolution of the worm. Equation (1) gives some basic relationships.

$$l_a = z_1 p_a \qquad p_a = \pi m_a \qquad m_a = \frac{m_n}{\cos\gamma} \qquad (1)$$

It is worth noting that there are three (3) expressions in Eq. (1) and should be interpreted as Eq. (1a), Eq. (1b), and Eq. (1c) from left to right. All other equations with multiple expressions should be interpreted, similarly. The definition of symbols can be in the nomenclature.

Worm threads are often specified by axial pitch. However, manufacturing may be easier and cheaper if standardized or preferred normal modules are used instead of standardized axial pitches because the gear could be made using spur gear hobs that have standardized modules.

Now, the lead angle of the worm and the helix angle of the gear is given in Eq. (2).

$$\gamma = \sin^{-1}\left(\frac{z_1 m_n}{d_1}\right) \qquad \psi = \gamma \qquad (2)$$

The lead angle may vary from 9° to 45° and a safe value of the lead angle is 12.5° according to [13]. It is

wise to limit lead angle to $6^{o}$ per thread [6, 14] for worms of multiple threads to minimize the difficulty of designing production tools and producing accurate curvature on worm threads and gear teeth. In the common wormset configuration where the shaft angle is $90^{o}$, the helix angle of the gear is equal to the lead angle of the worm as indicated in Eq. (2b) and they have the same hand [11].

The geometry of the worm gear is similar to that of a helical gear and its tooth proportions are chosen accordingly. The gear is throated in cylindrical worm sets so it can envelop the worm and provide for a greater area of contact. Throated gears require extremely precise mounting [11]. For helical gears, the pitch diameter may be construed as that of a nominal spur on the normal plane projected on the diametral plane. This relation is captured by Eq. 3a and Eq. 3b.

$$d_2^{/} = z m_n \qquad d_2 = \frac{d_2^{/}}{\cos \psi} \qquad d_2^{/} = d \cos \psi \qquad (3)$$

The speed ratio in wormsets is different from the gear ratio and is obtained as:

$$u = \frac{N_1}{N_2} = \frac{z_2}{z_1} \qquad (4)$$

The tangential velocity of the worm and that of the gear are not equal and are at right angles, creating slippage between the pitch cylinders of the worm and gear. The worm threads slide along the gear teeth similar to the threads of a screw sliding on those of the nut. The sliding velocity is:

$$V_s = \frac{\pi d_1 N_1}{60 \cos \gamma} \times 10^{-3} \qquad (5)$$

## 3. CONTACT RATIO AND LOAD SHARING FACTOR

### 3.1 Profile Planes

In a wormset, the axial plane of the worm corresponds to the transverse plane of the gear. Similarly, the axial plane of the gear corresponds to the transverse plane of the worm. However, the normal plane is common to both worm and gear. For ZN profile, $\phi_n$ is known, for ZA profile, $\phi_t$ is known, and Eq. (6) gives the relationship between these angles and the nominal helix angle which is defined by the lead angle of the worm.

$$\phi_t = \tan^{-1}\left[\frac{\tan \phi_n}{\cos \psi}\right] \qquad \phi_n = \tan^{-1}\left(\tan \phi_t \cos \psi\right) \quad (6)$$

According to Maitra [2], the base helix angle gives a more accurate estimate of the radius of curvature of the virtual or equivalent spur gear for a helical gear. Therefore, the plane defined by the base helix angle will be called the virtual plane on which the pitch diameter of the virtual spur gear for a helical gear lies. The instantaneous pitch diameter of the helical gear in the virtual plane during contact is given by Eq. (7a) [15].

$$d_v = \frac{d^{/}}{\cos^2 \psi_b} = \frac{d \cos \psi}{\cos^2 \psi_b} \quad \psi_b = \tan^{-1}\left[\tan \psi \cos \phi_t\right] \quad (7)$$

### 3.2 Load Sharing Factor

During gear transmission two (2) to three (3) gear teeth are claimed to be in contact with threads in wormsets [12]. An expression for the virtual contact ratio $\varpi_v$ s developed in Appendix A2 and is presented in Eq. (8). The virtual contact ratio as defined by Eq. (8a) will not yield a load sharing factor of 3 or above, especially for small values of gear teeth number and base helix angle ($\psi_b$) or lead angle. Therefore, there is a need to consider the influence of the worm threads on load sharing.

$$\varpi_v \approx \frac{\varpi_t}{\cos^2 \psi_b} \qquad \varpi_t = \frac{\kappa_1 + \kappa_2}{\pi \cos \phi_n} \qquad (8)$$

By considering the effective threaded length (Appendix A3) of the worm, a contact load sharing factor for worm drives may be defined as [16]:

$$\varpi_s = \varpi_v \lambda_c \qquad (9)$$

Refer to Appendix A4 for more discussion of these ideas on load sharing, worm contact coefficient, and contact effectiveness factor. The worm contact coefficient is estimated as [16]:

$$\lambda_c = \sqrt{\alpha_e(n_t - 2)z_1} \geq 1 \qquad n_t = \frac{b_1}{p_a} \qquad (10)$$

Generally, load sharing can be enhanced by wear-in and accurate manufacture of gear teeth. Low manufacturing accuracy and high hardness of gear teeth reduce load sharing. Inaccurate low-hardness gears may wear in and cold-flow enough to develop relatively good contact patterns and load shearing early in their service life [6]. This is usually the case in worm drives [12] where the worm is made substantially harder than the gear.

By considering a worm of a single thread and the above statements and equation, a value range of 0.4 to 1.0 was empirically established for $\alpha_e$. A conservative value of 0.45 seems reasonable for $\alpha_e$ and is adopted in this study (Please see Appendix A4).

The effective threaded length of the worm and the effective face width of the gear are expressed in Eq. (11a) and Eq. (11b), respectively [16].

$$b_1 = 2\sqrt{m_n(d_2 + m_n)} \quad b_2 = 2\sqrt{m_n(d_1 + m_n)} \quad (11)$$

## 4. CONTACT STRESS ESTIMATE

### 4.1 Model Formulation

As mentioned earlier, both pitting and scuffing are associated with contact stress, but the high sliding velocity in the mesh of wormsets makes scuffing a highly probable failure mode [11]. To minimize failure by scuffing, the contact stress is usually reduced based on the sliding velocity, with lower values used for higher velocities. Buckingham was the first person to investigate contact stresses in gear teeth in a systematic way [9]. He modified the Hertz contact stress express-ions for two frictionless cylinders in line contact to

study gear pitting resistance by defining the equivalent radii of curvature of the two cylinders in rolling contact. In helical gears, the actual contact between gear teeth and worm threads occurs in the virtual plane. Therefore, the contact force and geometric design parameters should be referred to as the virtual plane. The Hertz contact stress equation for line contact in helical gears is expressed as in Eq. (12) [17].

$$\sigma_H = \sqrt{\frac{F_{c2}E_c \times 10^3}{\pi \rho_v b_v \varpi_s}} \qquad E_c = \frac{2E_1E_2}{E_2(1-v_1^2) + E_1(1-v_2^2)} \qquad (12)$$

The contact force on the gear in the mesh depends on the tangential or transmitted force on the gear given in Eq. (13a).

$$F_{t2} = \frac{T_2 \times 10^3}{d_2} \qquad T_2 = \eta_w u T_1 \qquad (13)$$

From Appendix B6, the tangential force and normal contact force on the gear are related as shown in Eq. (14a).

$$F_{c2} = \frac{K_f F_{t2}}{\cos \phi_n \cos \psi} \qquad (14a)$$

where:

$$K_f = (1 + \vartheta_m)\left[1 - \frac{\vartheta_m \tan \psi}{\cos \phi_n}\right]^{-1} \qquad (14b)$$

The frictional load factor is given by Eq. (14b) and is derived in Appendix B6.

In the axial section, the sides of the worm profile are straight [1]. Therefore, the worm engages the gear as a helical rack [10]. A planar profile for the worm rack means mathematically, that it has an infinite radius of curvature. The instantaneous radius of curvature in the virtual plane during contact at the pitch point is [15]:

$$\rho_v = \frac{d_{v1}d_{v2}\sin \phi_n}{d_{v1} + d_{v2}} = \frac{d_{v2}\sin \phi_n}{1 + \frac{d_{v2}}{d_{v1}}} \qquad (15)$$

when $d_{v1} = \infty$, then from Eq. (15) and Eq. (7a):

$$\rho_v = d_{v2}\sin \phi_n = \frac{d_2\cos \psi \sin \phi_n}{\cos^2 \psi_b} \qquad (16)$$

Also:

$$b_v = \frac{b_e}{\cos \psi_b} \approx \frac{b_e}{\cos \psi} \qquad b_e = \lambda_e b \qquad (17)$$

The approximation of Eq. (17) is based on the throating provided on the gear which ensures an arc length contact, thereby increasing the effective contact surface.

Substitute Eqs. (8a), (9), (13a), (14a), (16) and Eq. (17) into Eq. (12a) to obtain:

$$\sigma_H = \frac{\cos^2 \psi_b}{d_2}\sqrt{\frac{K_g K_f T_2 E_c}{b_e \lambda_c \varpi_t \cos \psi}} \qquad K_g = \frac{2}{\pi \sin 2\phi_n} \qquad (18)$$

Eq. (18) is the theoretical contact stress capacity expression for cylindrical wormsets. But mathematical models are rarely if ever, able to depict exactly any physical system due to the simplifying assumptions incorporated. They are therefore, approximations and experiments are required in science and engineering to validate the models. Consequently, the theoretical model of Eq. (18) needs adjustment for a) service load influence factors, b) gear tooth profile modification, and c) effective contact width of gear face. When these factors are incorporated into Eq. (18), the engineering contact stress capacity model for cylindrical worm gears may be rendered as:

$$\sigma_H = \frac{\cos^2 \psi_b}{d_2}\sqrt{\frac{K_s K_g K_x T_2 E_c}{\lambda_e b \, \lambda_c \varpi_t \cos \psi}} \qquad (19)$$

Eq. (19) contains all the basic design parameters of the worm and gear and explicitly shows the influence of the parameters $\psi_b$, $\psi$, and $\lambda_c$. This is unique because no model available currently in the public domain has these terms.

The service load factor takes care of load excitations beyond the rated value that are reoccurring in nature, not the peak load which occurs only occasionally. It is estimated as:

$$K_s = K_a K_v K_m K_f K_w \qquad (20)$$

Refer to Appendix B for more explanations of how the component parameters of $K_s$ are evaluated for wormsets. The parameters $K_a$, $K_v$, and $K_m$ are empirical and are evaluated as in other types of gears based on AGMA recommendations, though there may be some modification sometimes. $K_f$ is a new semi-empirical parameter and is derived in Appendix B6. $K_w$ is a new empirical parameter, being introduced in this study. It applies only to wormsets and is empirically evaluated in Appendix B7, for different worm profiles. Another common modification to gear tooth profile is crowning that makes the contact patch more elliptical than rectangular and produces localized contact [9]. This leads to higher contact stresses at the points of contact, though it prevents edge contacts at the gear tips. The effect of crowning is accounted for by the crowning factor $K_x$ which may be taken as unity for cylindrical gears until definitive value(s) is established.

### 4.2 Acceptable Design

Eq. (19) is good for the design verification task as it predicts a contact stress value that can be compared with a permissible value. The acceptability of a design may be assessed by determining the apparent contact stress design factor. The estimated apparent contact stress design factor must be at least equal to the minimum allowable contact stress design factor. That is:

$$n_H = \frac{S_c}{\sigma_H} \qquad n_H \geq n_c \qquad (21)$$

$S_c$ is set by considering resistance to scuffing and seizure which is improved by increasing the surface hardness and surface finish of the threads of a worm [18]. The influence of the high sliding contact speed in

worm drives must be considered in the determination of $S_c$. Therefore, values of $S_c$ are usually lower than those used in cylindrical gears. The parameter $n_c$ is a minimum number that is considered to yield a safe and durable design and should be at least equal to unity. It may be prescribed by standards or codes or agreed on with a client before the design. In cylindrical and bevel gears, it is in the range of 1.0 to 1.3. Refer to Appendix C for a suggested estimate $S_c$ for bronze materials.

## 5. DESIGN EXAMPLES

This section presents the evaluation of the contact stresses of four design examples using the new contact stress capacity model of Eq. (19). The results obtained are compared with the previous values [1, 8, 20, 40]. The first two examples are based on GOST standards of the former Soviet Union. The third example is based on MITCalc [40] standard, a collection of engineering, manufacturing, and technical calculations. It is of European origin and is probably a modified version of ISO or a proprietary standard. The fourth example is based on DIN3999:2002 and is implemented in KISSsoft [20], gear design software that appears to be gaining in popularity. MITCalc [40] and DIN 3999:2002 [20] standards are newer than the GOST standards. The problem statements in the design examples have been paraphrased and the design parameters have been converted to metric units where necessary by the authors.

### 5.1 Example 1

A cylindrical worm drive delivers an output torque of 995 Nm when the gear shaft runs at 60 rpm. The speed ratio is 16.33, the gear pitch diameter is 343 mm and the pitch diameter of the worm is 77 mm. The gear has a nominal facewidth of 68 mm, while the worm has a nominal threaded length of 145 mm. The worm is made of hardened steel, has three threads with a lead angle of $15.25^0$, while the gear is made of phosphor bronze and is uncrowned. It is desired to calculate the contact stress on a gear tooth, assuming a ZN-type worm profile and a gear with a normal pressure angle of $20^0$ [8, pp. 357 – 360].

### 5.2 Example 2

A cylindrical worm drive provides an output torque of 836 Nm when the output shaft runs at 91.25 rpm. The speed ratio is 16, the gear pitch diameter is 320 mm and the pitch diameter of the worm is 80 mm. The gear has a nominal face width of 75 mm, while the worm has a nominal threaded length of 170 mm. The worm is made of hardened steel, has two threads with a lead angle of $13.19^0$, while the gear is made of phosphor bronze and is uncrowned. Similarly, to the situation in Example 1, computation of the contact stress on a gear tooth is sought, assuming a ZN type worm profile and a gear with a normal pressure angle of $20^0$ [1, pp. 429 – 434].

### 5.3 Example 3

A cylindrical worm drive delivers an output torque of 9948 Nm when the worm shaft runs at 1200 rpm. The speed ratio is 25, the gear pitch diameter is 483 mm and pitch diameter of the worm is 90 mm. The gear has a nominal face width of 77 mm, while the worm has a nominal threaded length of 98 mm. The worm is made of hardened steel, has three threads with a lead angle of $12.10^0$, while the gear is made of phosphor bronze and is uncrowned. Estimate the contact stress on a gear tooth, assuming a ZN-type worm profile and a gear with a normal pressure angle of $20^0$ [40].

### 5.4 Example 4

A worm-gear speed reducer provides an output torque of 588 Nm and a speed ratio of 20.5 using an electric motor running at 1500 rpm. Assume that the application factor is 1.0 and the gear is made from bronze with a yield strength of 180 MPa and nominal contact strength of 520 MPa [20]. The gear pitch diameter is 164 mm, the pitch diameter of the worm is 36 mm and the gear is uncrowned. Estimate the contact stress on a gear tooth, assuming a ZN type worm profile and a gear with a normal pressure angle of $20^0$ assuming a ZN type worm.

Table 1 is a summary of the input data from the problem statements. Table 2 shows some important intermediate design parameters evaluated using expressions in the sections above. Table 3 shows the percentage variances between the new contact stress estimates and those of previous results.

**Table 1: Input Data for Application Examples**

| Example | $T_2$ (Nm) | $d_2$ (mm) | $d_1$ (mm) | $u$ | $z_1$ | $b_g$ (mm) | $b_w$ (mm) |
|---------|-----------|-----------|-----------|-------|-------|-----------|-----------|
| 1 | 995 | 343 | 77 | 16.33 | 3 | 68 | 145 |
| 2 | 836 | 320 | 80 | 16.0 | 2 | 75 | 170 |
| 3 | 9948 | 483 | 90 | 25 | 3 | 77 | 98 |
| 4 | 588 | 164 | 36 | 20.5 | 2 | 31 | 60 |

**Table 2: Computed Data for Application Examples**

| Example | $b_2$ (mm)* | $b_1$ (mm)** | $K_s$ | $\varpi_v$ | $\lambda_c$ | $\varpi_s$ | $\Psi$ (Deg.) | $\psi_b$ (deg.) | $V_s$ (m/s) |
|---------|-------------|--------------|-------|-----------|------------|------------|---------------|-----------------|-------------|
| 1 | 48 | 95 | 1.317 | 1.829 | 1.940 | 3.549 | 15.25 | 14.31 | 4.10 |
| 2 | 60 | 110 | 1.298 | 1.797 | 1.291 | 2.320 | 14.05 | 13.19 | 6.30 |
| 3 | 50 | 73 | 1.231 | 1.873 | 1.616 | 3.028 | 12.10 | 11.35 | 5.80 |
| 4 | 25 | 51 | 1.183 | 1.826 | 1.481 | 2.705 | 12.53 | 11.75 | 2.90 |
| *Estimate from Eq. (11b). | | | | | **Estimate from Eq. (11a). | | | | |

**Table 3: Contact Stress Comparison for Examples**

| Example | Contact Stress (MPa) | | Variance (%) |
|---|---|---|---|
| | Current | Previous | |
| 1 | 150 | 157 | -4.46 |
| 2 | 163 | 164 | -0.61 |
| 3 | 351 | 350 | 0.29 |
| 4 | 368 | 367 | 0.29 |

## 6. DISCUSSIONS

### 6.1 Some Features of New Model

The new contact stress expression of Eq. (19) directly incorporates all the basic design parameters of the wormset. Specifically, parameters $K_g$, $\psi_a$, $\psi_b$, and $\lambda_c$ are unique in the expression because no model available currently in the public domain seems to have these terms. The parameter $\lambda_c$ is particularly important because it is used to capture the complex contact pattern between a worm thread and a gear. It depends on the number of worm threads $z_1$, the effective threaded length of the worm, $b_1$ the axial pitch $p_a$, and the contact effectiveness factor $\alpha_e$. It is only $\alpha_e$ that is new and was estimated in a semi-empirical way in Appendix A4. The other empirical parameters in the model are $\lambda_e$, $K_s$ and $K_x$. But the component parameters of $K_s$ are estimated using the same methods for cylindrical or bevel gears. The parameter $K_g$ has derived analytically, while $K_f$ is derived semi-empirically, but it is a component of $K_s$.

The composite elastic modulus ($E_c$) needed in Eq. (19), for steel and bronze materials is 160 GPa [17]. The parameter $K_w = 1.0$ (for ZN worm profile) is assumed in all the design cases considered. The external load application factor $K_a$ is set to unity since it was unspecified in examples 1 to 3 but stated to 1.0 in example 4. $K_x = 1$ in the examples as the gears are uncrowned.

### 6.2 Application Examples and Comparisons

Four wormset designs from different references were used to test the new contact stress model. In using the new contact stress model, the normal module, the pitch diameter of the worm, and the pitch diameter of the gear are kept the same as in the references. The effective threaded length of the worm and the effective face width of the gear were calculated as indicated by Eq. (11) for all examples. This was done to ensure that the derived new parameters in the current model were used in determining the contact stress. Also, the service load factor was evaluated for each example as described in Appendix B. These actions were informed by the need for consistency in applying the new model and ensuring that the approach being presented may be judged on its merit.

Table 2, column 4 shows the values of $K_s$ determined for the Examples. These values are relatively low, as would be expected for more quiet drives like wormsets. Table 2, column 5 gives values of the virtual contact ratio, which are observed to be near or above 1.80, depending on the number of teeth on the gear. The values of the worm contact coefficient in column 6 indicate the increase in load sharing resulting primarily from the use of multiple threads and secondarily from the number of gear teeth in the active threaded length of the worm. It was first used in worm drive design in [16] and it appears there is no similar parameter in the stress models in the cited references and current worm design standards.

Table 2 column 7 shows the load sharing factor. In problem Example 1, this column indicates that 3 or 4 teeth are in contact with the worm screw during load transmission. This is possible since there are three threaded pathways for the gear teeth, and they are radially out of phase by $120^0$. At the beginning of a revolution, one tooth is engaged in the first thread, after the worm turns through $120^0$, the second thread takes another gear tooth, so two teeth are now in the mesh. When the worm rotates $240^0$, the third thread takes the third gear tooth. Therefore, between $240^0$ and $360^0$ rotations all three teeth are in the worm threads. As the first gear tooth exits the worm, the fourth tooth is entering engagement in the first thread. Thus, a minimum of three gear teeth are in active engagement with the worm at any time with unequal load distribution or sharing per tooth. The wormset of Example 3 operates similarly to that of Example 1. Examples 2 and 4 worms have two threaded pathways for the gear teeth which are radially out of phase by $180^0$. At the beginning of a revolution, one tooth is engaged in the first thread, after the worm turns through $180^0$, the second thread takes another gear tooth, so two teeth are now in the mesh. As the first gear tooth exits the worm, the third tooth is entering engagement in the first thread. Hence, a minimum of two gear teeth are in active engagement with the worm at any time.

A comparison of columns 8 and 9 in Table 2 indicates that the base helix angle trails the nominal helix angle. The difference between the two is marginal at low values of the nominal helix angle but increases with higher values of the helix angle. The base helix angle helps in reducing the contact stress in helical gears and the reduction is more pronounced at high values (Eq. (19)). The last column of Table 2 shows the sliding speed in the wormsets which is used to estimate the internal dynamic overload factor, mesh friction and the velocity factor for the pitting strength.

Table 3 compares the contact stress estimates from the current model with previous solutions. Table 3 column 2 shows the estimated contact stress from the present model while column 3 shows the previous results. Table 3 column 4 shows the percentage variances between the current and previous results. The variances between the present model and previous results are approximately between -4.5% and 0.3%. The negative variances show that the new model estimates are lower than the previous values, while positive variances show the new model values are higher than the previous values.

It should be noted that an average value of 0.85 was chosen for $\lambda_e$ based on a comparison of wormset and bevel gear shaft lateral rigidity. Now, a value of 0.8 will be on a more conservative side, but because the estimated contact stresses from the new model for

examples 3 and 4 are very favorable when compared with the previous result, using a value of 0.85 for $\lambda_e$ in the current contact stress capacity model appears justified.

The values of the variances in Table 3 attest to near excellent comparison, indicating that the new model predictions may be trusted with some confidence. Therefore, the new model is suggested as sufficiently accurate for preliminary sizing and verification of cylindrical wormsets.

## 6.3 Apparent Pitting Design Factor

Design adequacy is commonly addressed by requiring a minimum safety or design factor and or specifying a reliability level as indicated by Eq. (21). The gear material and pitting strength must be known for Eq. (21) to be useful. No specific bronze material is mentioned for the gears in Examples 1 and 2. A popular material used for most worm gears is C90700 (SAE 65) phosphor bronze [11, p. 567] and is assumed these Examples. The worm gears are assumed to be made by casting using C90700 material, which has a yield strength of 152 MPa and tensile strength of 303 MPa [38]. The material for Examples 3 and 4 has a yield strength of 180 MPa and tensile strength of 300 MPa [20, 40]. The nominal strength of materials is usually specified at 99% reliability and is assumed in the estimation of the nominal pitting strength of bronze materials for the design Examples. Please, refer to Appendix C, where the service pitting strength for the Examples was evaluated.

**Table 4: Apparent Pitting Design Factor for Examples**

| Example | $S_c$ (MPa) | $\sigma_H$ (MPa) | $n_H$ |
|---------|-------------|------------------|-------|
| 1 | 330 | 150 | 2.20 |
| 2 | 315 | 163 | 1.93 |
| 3 | 371* | 351 | 1.06 |
| 4 | 410 | 367 | 1.12 |
| *Size factor of 0.97 applied [40] | | | |

Table 4 shows the contact stress and the apparent pitting design factor. The apparent pitting design factor is given in the last column of Table 4. Eq. (21) requires an apparent pitting design factor of unity as a minimum and from the last column of Table 4; this condition is satisfied in all the Examples. The apparent design factor in the previous solutions for Examples 3 and 4 are 1.03 and 1.2, respectively. In the current solutions, the values are respectively, 1.06 and 1.12. Therefore, the current solution appears slightly more conservative for Example 3 and slightly less conservative for Example 4. The apparent design factors for Examples 1 and 2 are around 2.0, which seem relatively high. As indicated earlier, the minimum apparent pitting design factor range is 1.0 to 1.3 for cylindrical and bevel gears, but worm gears are more complicated. Therefore, values of apparent pitting design factor above 1.5 for worm gears may probably be too high and should call for design review/revision.

It would have been a good idea to use a material with lower mechanical strength properties for Examples 1 and 2, to reduce the apparent pitting

strength design factor. But it must be noted that the sliding velocities are rather a concern in these cases. An alternative would have been to keep the material but reduce the normal module, thus reducing the worm pitch diameters for these Examples and recalculating other sizes and contact stress. This would increase the contact stress and reduce the apparent design factor. Such a measure would lead to reduced costs for the bronze material.

The internal dynamic overload factor for wormsets is predicted by modifying that of spur gearsets in this presentation. Also, the mesh overload factor for wormsets is predicted from shaft lateral rigidity comparison with straddle mounted bevel gears. These approaches appear to yield reasonable results considering the good agreement between the new model and previous results. Therefore, a unified and consistent method of evaluating these parameters for all kinds of gears appears to have been established. However, the evaluation of the mesh overload factor deserves further investigation, especially at the experimental level so that the validity of the approach can be confidently established.

## 7. CONCLUSIONS

A contact stress expression is derived for cylindrical wormsets by considering the worm as a helical rack mating with a helical gear. The concept of the equivalent spur gear for a helical gear defined by the instantaneous radius of curvature in the virtual plane of the helical gear is utilized in the contact stress capacity model formulation. The virtual plane is defined by the base helix angle and is different from the normal plane which is defined by the nominal helix angle. According to Maitra [2], the instantaneous radius of curvature of the equivalent spur gear is estimated more accurately on the virtual plane.

The new contact stress capacity model utilizes all the basic design parameters of worm and gear, explicitly showing the influence of the base helix angle and nominal helix angle on the contact stress. By considering the geometry of the worm and gear in engagement, active gear facewidth and active threaded length of the worm are defined. The influence of the number of active gear teeth over the active threaded length of the worm in the axial plane is incorporated in a new parameter introduced in the model, an aspect not considered in other formulations. The model also accounts for multiple threaded worms which seem not to have been treated till now. The service load factor expression for cylindrical gears is modified to take account of different thread profile designs in worm sets and the influence of mesh friction.

Contact stress computations of wormset designs for four examples from different references were carried out using the current model. In Table 3, the variances between the contact stress estimates from the new wormset contact stress model and the previous results are in the range of -4.5% to 0.3%. These seem to indicate very good correlations with the previous estimates. Certainly, more examples are necessary for further verification of the design approach presented.

However, it appears that the approach is sufficiently accurate enough to be acceptable for the preliminary design of cylindrical wormsets because DIN3999:2002 is a well-established design standard. Consequently, it seems that a reliable and more analytical method for cylindrical worm drive design has emerged. Official design validation must be conducted according to a contractual agreement between the designer and the client. This may require compliance with ISO 6336, ANSI/ AGMA 2001-D04, DIN3999:2002, or any other relevant gear design standards.

**ACKNOWLEDGEMENTS**

**NOMENCLATURE**

| | |
|---|---|
| 1 | subscript for worm |
| 2 | subscript for gear |
| HVN | Hardness: Vicker's number |
| $a_1$ | AGMA velocity exponent |
| $a_2$ | AGMA velocity coefficient |
| $b$ | minimum nominal facewidth of gearset (mm) |
| $b_1$ | active threaded length of worm (mm) |
| $b_2$ | active facewidth of gear |
| $b_e$ | effective facewidth of gear (mm) |
| $b_g$ | nominal facewidth of gear |
| $b_w$ | nominal threaded length of worm (mm) |
| $b_v$ | gear facewidth on the virtual plane (mm) |
| $d$ | helical gear pitch diameter (mm) |
| $d_1$ | worm pitch diameter (mm) |
| $d_2$ | pitch diameter of nominal spur gear (mm) |
| $d_2$ | pitch diameter of helical gear (mm) |
| $d_v$ | pitch diameter of virtual gear (mm) |
| $E_c$ | composite or effective elastic modulus (GPa) |
| $E$ | elastic modulus of pinion or gear material (GPa) |
| $F_a$ | axial force (N) |
| $F_c$ | normal contact force (N) |
| $F_r$ | radial force (N) |
| $F_{t2}$ | transmitted (tangential) force on gear tooth(N) |
| $F_{c2}$ | normal contact force on gear tooth (N) |
| $h_a$ | rack addendum (mm) |
| $h_t$ | gear tooth whole depth (mm) |
| $k_p$ | plane strain factor |
| $k_w$ | work-hardening factor |
| $K_a$ | application or external overload factor |
| $K_b$ | bevel load factor |
| $K_f$ | mesh frictional load factor |
| $K_g$ | contact stress form factor |
| $K_m$ | mesh overload factor |
| $K_{mf}$ | mesh frictional load factor |
| $K_{tf}$ | thread frictional load factor |
| $K_o$ | basic internal dynamic overload factor |
| $K_p$ | tooth profile modification load factor |

| | |
|---|---|
| $K_r$ | rim flexibility load factor |
| $K_s$ | service load factor |
| $K_v$ | internal dynamic overload factor |
| $l_a$ | axial lead (mm) |
| $l_{v1}$ | length of approach for rack gear on the virtual plane |
| $l_{v2}$ | length of recess for gear on the virtual plane |
| $m_a$ | axial module (mm) |
| $m_n$ | normal module (mm) |
| $n_H$ | apparent pitting design factor |
| $n_c$ | minimum pitting design factor |
| $n_t$ | number of gear teeth on effective threaded length of the worm |
| $N_1$ | rotational speed of pinion or gear (rpm) |
| $p_a$ | axial pitch (mm) |
| $P_1$ | transmitted power by driving gear (kW) |
| $r_v$ | pitch radius of virtual gear (mm) |
| $r_{v2}$ | pitch radius of virtual worm gear (mm) |
| $S_{yc}$ | compressive yield strength (MPa) |
| $S_{yt}$ | tensile yield strength (MPa) |
| $S^*_c$ | theoretical pitting strength (MPa) |
| $S'_c$ | nominal pitting strength (MPa) |
| $S_c$ | service pitting strength (MPa) |
| $S_H$ | permissible or allowable pitting stress (MPa) |
| $t_r$ | rim thickness (mm) |
| $T$ | transmitted torque (Nm) |
| $T_1$ | torque transmitted by driving gear (Nm) |
| $T_2$ | torque transmitted by driven gear (Nm) |
| $u$ | speed ratio |
| $V_s$ | sliding velocity (m/s) |
| $V_t$ | tangential velocity at pitch point (m/s) |
| $z$ | physical number of teeth on gear or pinion |
| $z_1$ | number of threads on worm |
| $z_{i1}$ | number of diametral teeth on the involute worm |
| $z_v$ | virtual number of gear teeth |
| $z_{v1}$ | number of virtual teeth on the involute worm |
| $Z_c$ | effective pitting strength adjustment factor |
| $Z_n$ | pitting durability adjustment factor |
| $Z_r$ | pitting reliability adjustment factor |
| $Z_x$ | pitting size adjustment factor |
| $Z_v$ | pitting sliding velocity adjustment factor |
| $\alpha_e$ | contact effectiveness factor |
| $\alpha_m$ | material friction factor |
| $\kappa_1$ | approach length factor |
| $\kappa_2$ | reccess length factor |
| $\lambda_e$ | effective facewidth factor |
| $\sigma_H$ | maximum Hertz contact stress (MPa) |
| $\phi_n$ | normal pressure angle (deg.) |
| $\phi_t$ | transverse pressure angle (deg.) |
| $\phi_{wt}$ | working transverse pressure angle (deg.) |
| $\phi_{wn}$ | working normal plane pressure angle (deg) |
| $\rho_v$ | instantaneous radius of curvature on a virtual plane at pitch point (mm) |
| $Y$ | Poisson's ratio of pinion or gear material |
| $\vartheta_m$ | mesh friction coefficient |
| $\lambda_r$ | rim backup ratio |
| $\eta_w$ | worm efficiency |
| $\gamma$ | worm lead angle (deg.) |
| $\varpi_v$ | contact ratio on the virtual plane |

| | |
|---|---|
| $\varpi_t$ | transverse contact ratio |
| $\varpi_s$ | load sharing factor |
| $\lambda_c$ | worm contact coeficient |
| $\psi$ | helix angle of gear (deg.) |
| $\psi_b$ | base helix angle of gear (deg.) |
| $b_v$ | gear facewidth on the virtual plane (mm) |
| $\upsilon$ | Poisson's ratio |
| $\eta_w$ | wormset efficiency |

## REFERENCES

[1] Berezovsky, Y., Chernilevsky, D. and Petrov, M., *Machine Design*, MIR Pub., Moscow, 1988.

[2] Maitra, G. M., *Fundamentals of Toothed Gearing: Handbook of Gear Design*, 2nd Edition, McGraw Hill, New Delhi, 2013.

[3] Winsmith, *The Speed Reducer Book: A Practical Guide to Enclosed Gear Drives*, Peerless-Winsmith, Springville, U.S.A, 1980.

[4] Brown, M. D., *Design and Analysis of a Spiral Bevel Gear,* Master's Thesis, Rensselaer Polytechnic Institute, Hartford, Connecticut, USA, 2009.

[5] Walsh, R. A., *Electromechanical Design Handbook*, 3rd ed. McGraw Hill, New York, 2000.

[6] Dudley, D. W., *Handbook of Practical Gear Design*, CRC Press, 2004.

[7] Shigley, J. E. and Mischke, C. R., *Standard Handbook of Machine Design,* 2nd Edition, McGraw-Hill, 1996.

[8] Dobrovolsky, Zablonsky, K., Mak, S., Radchik, A., Erlikh, L. *Machine Elements*, Foreign Lan–guage Pub. House, Moscow, 1965.

[9] Norton, R. L., *Machine Design: An Integrated Approach*, 2nd. Edition, Prentice-Hall, Upper Saddle River, New Jersey, 2000.

[10] Collins, J. A., Busby, H., Staab, G. H., *Mechanical Design of Machine Elements and Machines: A Failure Prevention Perspective,* 2nd ed., John Wiley and Sons, New York, 2010.

[11] Juvinall, R. C. and Marshek, K. M., Juninall's *Fundamentals of Machine Component Design*, SI, Wiley, Singapore, 2017.

[12] Schmid, S. R., Hamrock, B. J. & Jacobson, B. O., *Fundamentals of Machine Elements*, 3rd ed., CRC Press, New York, 2014.

[13] Khurmi, R. S. & Gupta, J. K., *A Textbook of Machine Design*, Eurasia Pub. House, New Delhi, 2015.

[14] Bhandari, V. B., *Design of Machine Elements*, 3rd ed. McGraw-Hill, New Delhi, 2010.

[15] Osakue, E. E. and Anetor, L, *Helical Gear Contact Fatigue Design by Spur Gear Equivalency*, Int'l Journal of Research in Engineering and Technology, Vol. 06, Issue 02, 2017.

[16] Osakue, E. E. and Anetor, L., *Design Sizing of Cylindrical Worm Gearsets*, FME Transactions, Vol. 48, No 1, pp. 31 - 45, 2020; doi:10.5937 /fmet2001031O.

[17] Osakue, E. E., *Simplified Spur Gear Design*, Proceedings of International Mechanical Engineering Congress and Exposition 2016 IMECE, Paper Number IMECE2016-65426, November 11-17, Phoenix Arizona, USA, 2016.

[18] Chernilevsky, D., *A Practical Course in Machine Design*, MIR, Moscow, 1990.

[19] Cherlivevsky, D. Lavrova, E. and Romanov, V., *Mechanics for Engineers*, MIR, Moscow, 1984.

[20] KISSsoft Tutorial 16, *Analysing the Geometry of Cylindrical Worm Gears with Enveloping Worm Wheel*;https://old.kisssoft.ag/english/downloads/pdf/03-17/kisssoft-tut-016-E-wormgear.pdf, (Accessed May 16, 2021).

[21] Budynas, R. G. & Nissbett, J. K., Shigley's *Mechanical Engineering Design, 9th Edition*, McGraw Hill Education, 2010.

[22] ANSI/AGMA 2005-D03, *Design Manual for Bevel Gears*; http://allaboutmetallurgy.com/wp/wp-content/uploads/2016/12/Design-Manual-for-Bevel-Gears.pdf, 2005, (Accessed March 20, 2021). content/uploads/2016/12/Design-Manual-for-Bevel-Gears.pdf, 2005, (Accessed March 20, 2021).

[23] DET NORSKE VERITAS, (2003), *Calculation of Gear Rating for Marine Transmissions*, Classification Notes, No. 41.2, 2003, https://rules.dnvgl.com/docs/pdf/DNV/cn/2012-05 /CN41-2.pdf, (March 10, 2021).

[24] Bhadari, V. B., *Design of Machine Elements*, 3rd ed. McGraw Hill Education (India), New Delhi, 2010.

[25] Hannah J., Stephens R. C., *Mechanics of Machines: Advanced Theories and Examples,* Edward Arnold, London, 1979.

[26] Kapelevich, A., *Direct Gear Design*, CRC Press, Baca Raton, U.S.A.

[27] *Elements of Metric Gear Technology*, http://qtcgears.com/tools/catalogs/PDF_Q420/Tech.pdf , Hicksville, NY, USA. (Accessed August, 2021).

[28] KHK, *Calculations of Gear Dimensions*; https:// khkgears.net/new/gear_knowledge/gear_technical _reference/calculation_gear_dimensions.html, Kohara Gear Industry Co., Ltd., Saitama-ken, 332-0022, Japan. (Accessed August, 2020).

[29] Framo, *Worm Gear Sets*, www.framo-morat.com, (Accessed August 2021).

[30] Childs, P. R. N., *Worm Gears: Mechanical Design Engineering Handbook*, Butterworth Heinemann Elsevier, Boston, Chap. 11, 2014.

[31] Mott, R. L., *Machine Elements in Mechanical Design*, 4th Edition, Pearson, Prentice-Hall, Singapore, 2006.

[32] RoyMech: *Gears-Gear Efficiency*, www.roymech. co.uk/Useful_Tables/Drive/Gear_Efficiency.html, (Accessed August 2021).

[33] Gope, P. C., *Machine Design: Fundamentals and Applications*, PHI Learning Private Limited, New Delhi, 2012, p. 98.

[34] Gearmotion: *Advantages of Worm Gears*, Syracuse, NY 13209 USA, https://gearmotions .com/advantages-of-worm-gears/,

[35] Osakue, E. E. and Anetor, L., *A Comparative Study of Contact Stress from Different Standards for Some Theoretical Straight Bevel Gear Pairs*, Int'l Journal of Research in Engineering and Technology, Vol. 07, Issue 8, 2018.

[36] Osakue, E. E. and Anetor, L., *Comparing Contact Stress Estimates of Some Straight Bevel Gears with ISO 10300 Standards*, Proceedings of International Mechanical Engineering Congress and Exposition 2016 IMECE, Paper Number IMECE2018-86573, November 9-15, Pittsburgh, Pennsylvania, USA, 2018.

[37] Akira Ishibashi, Shigeru Hoyashita, Hidehiro Yoshino, *Studies on Upper Limit of Surface Durability of Phosphor Bronze*, Bulletin of JSME, Vol. 27 (1984) No. 225 P 592-600, 1984; http://doi.org/10.1299/jsme1958.27.592

[38] SAE 65, *Gear Bronze*; https://www.national bronze.com/C90700_Gear_Bronze.php (6-17-21).

[39] Edward E. Osakue, Anetor, L. and Harris, K., *Pitting Strength Estimate for Cast Iron and Copper Alloy Materials*, FME Transactions (2021) 49, 269-279; doi:10.5937/fme2102269O.

[40] MITcalc - *Worm gear, geometric design and strength check*; https://www.mitcalc.com/en/ui/worm gear.pdf.

[41] Edward E. Osakue, Anetor, L. and Harris, K., A *Parametric Study of Frictional Load Influence in Spur Gear Bending Resistance*, FME Transactions journal, (2020) 48, 294 – 306.

## APPENDIX A: WORMSET SPECIAL ISSUES

### A1 Effective Facewidth Factor

Ideally, the contact patch in gear drives should envelop the complete tooth mesh surface, but practically this may not happen. Factors such as thermal gradient, centrifugal forces, work hardening, residual stresses [21], etc. can distort pinion or gear shape and lead to teeth mismatch that could impact contact quality. The effective face width of gear may be expressed as:

$$b_e = \lambda_e b \qquad b = \min(b_1, b_2) \qquad (A1)$$

The expected range of values for $\lambda_e$ is 0.80 to 0.90 for bevel gears, with an average of 0.85 [22, 23].

Since wormsets are designed with similar lateral rigidity as bevel gears [1], it may be assumed that the value of $\lambda_e$ for wormsets is in the same range as for bevel gears. The approximation of the arc of face contact for throated gears [24, 1] with a straight line

(Eq. (17a)) makes the facewidth contact length estimate conservative. Therefore, an overly conservative value of $\lambda_e$ may not be necessary. Hence a value of 0.85 for $\lambda_e$ is adopted for cylindrical worm gears in this study.

### A2 Virtual Contact Ratio

Two types of contact ratios may be associated with worm drives and they are the virtual plane and transverse plane contact ratios. The contact ratios are based on the addendum diameters of the gears in the virtual and transverse planes, respectively. The virtual plane contact ratio is defined as:

$$\varpi_v = \frac{l_{v1} + l_{v2}}{\pi m_n \cos \phi_n} \qquad (A2)$$

For worms with a trapezoidal section in the axial plane, a helical rack-pinion engagement takes place between the worm and the gear.

In an ordinary spur gear-rack system, the length of approach for a rack gear is equal to the rack gear addendum divided by the sine of the pressure angle [2, 25]. Therefore, the length of approach for the rack gear with a trapezoidal section in the virtual plane is then:

$$l_{v1} = \frac{h_a}{\cos^2 \psi_b \sin \phi_n} = \frac{m_n}{\cos^2 \psi_b \sin \phi_n} \qquad (A3)$$

In the case of a worm with a trapezoidal profile [2, 25]:

$$l_{v1} = \frac{m_n \kappa_1}{\cos^2 \psi_b} \qquad \kappa_1 = \frac{1}{\sin \phi_n} \qquad (A4)$$

In the case of a worm with an involute profile, the virtual number of teeth on the worm is presented by Eq. (A5) [26, p. 58].

$$z_{v1} = \frac{z_1}{\sin^3 \psi_b} \qquad (A5)$$

Based on Eq. (A5), Eq. (A4b) becomes:

$$\kappa_1 = 0.5 \left( \sqrt{(z_{v1} + 2)^2 - (z_{v1} \cos \phi_n)^2} - z_{v1} \sin \phi_n \right) \cos^2 \psi_b \qquad (A6)$$

The length of recess for the gear is:

$$l_{v2} = \sqrt{(r_{v2} + m_n)^2 - (r_{v2} \cos \phi_n)^2} - r_{v2} \sin \phi_n \qquad (A7a)$$

$$l_{v2} \approx \frac{0.5 m_n}{\cos^2 \psi_b} \left( \sqrt{(z_2 + 2)^2 - (z_2 \cos \phi_n)^2} - z_2 \sin \phi_n \right) \qquad (A7b)$$

Eq. (A7b) can be expressed as:

$$l_{v2} = \frac{m_n \kappa_2}{\cos^2 \psi_b} \qquad (A8a)$$

where:

$$\kappa_2 = 0.5 \left( \sqrt{(z_2 + 2)^2 - (z_2 \cos \phi_n)^2} - z_2 \sin \phi_n \right) \qquad (A8b)$$

Combining, Eqs. (A2), (A4) or (A6), and (A8):

$$\varpi_v \approx \frac{\varpi_t}{\cos^2 \psi_b} \qquad \varpi_t = \frac{\kappa_1 + \kappa_2}{\pi \cos \phi_n} \qquad (A9)$$

It should be noted that Eq. (A4b) for trapezoidal worms will yield a higher value than Eq. (A6) for involute worms, indicating that trapezoidal worms may experience slightly lower contact stress for the same load.

## A3 Effective Threaded Worm Length and Gear Facewidth

According to Dudley [6] and Shigley and Mischke [7], the useful portion of a worm gear facewidth is obtained if a tangent line is drawn to the worm pitch circle diameter to intersect the tip or outside circle diameter of the worm. This geometric description leads to Eq. (A11a) for the useful or effective facewidth of the gear and is considered to be always safe [16].

The effective threaded length of a worm may be derived from a similar logic. That is, the active portion of the threaded length of the worm is defined by a tangent line to the gear pitch circle diameter intersecting the gear tip or outside circle diameter. This relationship results in Eq. (A11b) for the worm [16].

$$b_2 = 2\sqrt{m_n(d_1 + m_n)} \quad b_1 = 2\sqrt{m_n(d_2 + m_n)} \qquad (A10)$$

According to Schmid et al. [12], a threaded worm length of 5 axial pitches is reasonable and allows one axial pitch before and after the contact zone. This means two axial pitches may be added to the effective length of a worm. Therefore, from Eq. (A10b), the nominal threaded length of the worm may be estimated by Eq. (A11a). The nominal facewidth of gear is assumed to be approximately given by Eq. (A11b).

$$b_w = b_1 + 2p_a \qquad b_g \geq b_2 + m_n \qquad (A11)$$

But there are other empirical alternatives to Eq. (A11a) such as $b_1$ being increased by 25 to 30 mm for the feed marks produced by the vibrating grinding wheel as it leaves the thread root [13]. Chernilevsky [18] suggests adding 25 mm for $m_a > 10$ mm, 35 to 40 mm for 10 mm $\leq m_a \leq 16$ mm, and 50 mm for $m_a > 16$ mm based on manufacturing considerations. Berezovsky et al. [1] suggest adding 3 $m_a$ to $b_1$ or hobbed and ground worms. Therefore, a minimum manufacturing allowance of about 25mm is expected for most cylindrical wormsets. From the foregoing considerations, Eq. (A11a) is the preferred choice in this study for estimating the nominal threaded length of a cylindrical worm because it would potentially yield a more consistent estimate.

## A4 Worm Contact Coefficient and Effectiveness Factor

This section considers two new parameters in wormset design: namely worm contact coefficient and worm contact effectiveness factor. The parameters are used to characterize the complex interaction between worm and gear during operation.

### A4.1 Worm Contact Coefficient

In the axial plane of the worm, several gear teeth may be spanned by the effective threaded length of the worm but the first and last gear teeth in the effective portion of the thread usually make partial contact with a worm thread. In the axial section of the gear, gear tooth contact on the face of a thread is a series of arcs [1] of varying length described by successive gear teeth from the base circle radius to the addendum circle radius. The arcs are initiated as line contacts, but as the gear and worm rotate, the contact lines develop into curves resulting in a highly unequal load distribution along the thread length as the gear face width is increased [6, 10, 12]. The effective length of contact is then a summation of these arcs described by each gear tooth in mesh with a worm thread, but they are mathematically complex in the description. To address this complexity, two parameters are introduced: worm contact coefficient and worm contact effectiveness factor.

The worm contact coefficient is expressed as [16]:

$$\lambda_c = \sqrt{\alpha_e(n_t - 2)z_1} \geq 1 \qquad (A12)$$

### A4.2 Worm Contact Effectiveness Factor

As mentioned earlier, the nominal threaded length of a worm may be estimated using Eq. (A11a) and allows one axial pitch before and after the contact zone. When Eqs. (9b) and (A11a) are combined, then:

$$b_w \approx (n_t + 2)p_a \qquad (A13)$$

One popular empirical estimate of the nominal threaded length of the worm is [27, 28]:

$$b_w = p_a(4.5 + 0.02z_2) \qquad (A14)$$

By comparing Eqs. (A13) and (A14):

$$n_t = 2.5 + 0.02z_2 \qquad (A15)$$

According to Dudley [6, p. 3.68], the number of $z_2$ should not be less than 29 and Petrov et al. [1], suggest a value of 28 for $z_2$ as about the minimum. Worm gear tooth failure in bending is rare but may occur in small module gears when gear teeth number is high, say 100 or more [1]. Therefore, power transmission wormsets are unlikely to have $z_2 > 100$. Also, it should be noted that low values of $z_2$ are associated with multiple start threads in Eq. (A12). Hence, assuming $z_2$ is between 28 and 100, then, $n_t$ is between 3.06 and 4.5 from Eq. (A15).

The worm contact effectiveness factor ($\alpha_e$) is assumed to accounts for the summation of the series of arcs of contact between the gear teeth faces and worm threads. Assuming $z_1 = 1$ in Eq. (A12); then $0.4 \leq \alpha_e \leq 1.0$ for $n_t$ between 3.06 and 4.5 estimated above. A conservative value of 0.45 for $\alpha_e$ is chosen for the current analysis.

### A5 Wormset Efficiency

Worm gearset efficiency is relatively low compared to other gear types, therefore, power loss cannot be

assumed negligible during transmission. During operation, the worm threads slide on the worm gear teeth in much the same manner that the threads of a screw slide along the surfaces of a nut in a screw mechanism. The lower efficiency results from the high sliding velocity between the mating surfaces of the worm and gear. During run-in, the softer gear teeth surfaces are work-hardened by the harder worm thread surfaces. The work-hardened gear surfaces also, become smoother, reducing friction by up to 15%, [10]. However, starting friction in wormsets may be up to 30% higher, [29]. The efficiency of the worm is [30, 31]:

$$\eta_w = \frac{\cos\phi_n - \vartheta_m \tan\gamma}{\cos\phi_n + \vartheta_m \cot\gamma} \quad \gamma = \sin^{-1}\left[\frac{z_1 m_n}{d_1}\right] \quad (A17)$$

Assuming case-hardened ground steel worm mating with quality phosphor bronze gear that is copiously lubricated, the mesh friction coefficient may be approximated as [32]:

$$\vartheta_m = \frac{0.04\alpha_m}{V_s^{0.25}} \leq 0.15\alpha_m \quad (A18)$$

Table A1 shows suggested values of $\alpha_m$.

For through-hardened and unground worm, the mesh friction value is approximately 25% higher than that predicted in Eq. (A18) above. The higher tangential speed of the worm facilitates the formation of an oil wedge in the contact area, resulting in lower frictional losses [1]. When the sliding speed is less than 3 m/s, the mesh friction value in Eq. (A18) may be increased by 25%. A typical value of the friction coefficient in wormsets is 0.05 [7, 30].

**Table A1: Material Friction Factor, [31]**

| Worm Material | Gear Material | Material Factor ($\alpha_m$) |
|---|---|---|
| Case-hardened steel | Phosphor bronze | 1.00 |
| | Aluminum bronze | 1.15 |
| | Cast iron | 1.20 |

### Appendix B: Service Load Factor

The service load factor takes care of load excitations beyond the rated value that are reoccurring in nature, not the peak load which occurs only occasionally. It represents a magnification factor that is used to approximately capture the load increase on gear due to manufacturing, assembly, and installation deficiencies and other operating factors influencing service loads. In general, the service load factor for wormsets may be estimated as:

$$K_s = K_a K_v K_m K_r K_f K_p K_w \quad (B1)$$

### B1 Application Factor, $K_a$

The external overload or application factor accounts for probable load variations arising from the accelerations and or decelerations of the connected masses of the power source device and the driven or load device. It can only be established after considerable field experience in a particular field. Many industries have established suitable values based on experience [17]. AGMA has recommended external overload for the design of gear reducers and references can be made to them. Generally, values recommended for wormsets are usually lower than those for cylindrical or bevel gears.

### B2 Internal Overload Factor, Kv

The dynamic or internal overload factor may be estimated based on AGMA recommendations for spur gears which can be modified for helical gears. For spur gears and based on the tooth profile manufacturing quality ($q_n$), the internal overload factor is approximated as in Eq. (B3a).
For, $6 \leq q_n \leq 12$:

$$a_1 = 0.25(q_n - 5)^{2/3} \quad a_2 = 3.5624 + 4(1 - a_1) \quad (B2)$$

$$K_o = \left[1 + \frac{\sqrt{V_s}}{a_2}\right]^{a_1} \quad V_s = \frac{\pi N_1 d_1 \times 10^{-3}}{60\cos\psi} \quad (B3)$$

Now, a worm gear is a helical gear and according to Maitra [2], the internal load in helical gears is about 75% of those for spur gears. Since worm gears are known to be the quietest gear drives [5], even quieter than helical gears, it would be conservative to assume that they experience about the same level of internal dynamic overload as helical gears. Therefore, the internal dynamic overload factor for wormsets may be approximated as [15]:

$$K_v = 1.0 + 0.75(K_o - 1) \quad (B4)$$

To facilitate run-in, worm gears should preferably be made to premium quality gear profile grade [16] by ensuring that $1.15 \leq K_v \leq 1.25$.

### B3 Mesh Overload Factor, $K_m$

The mesh overload factor, $K_m$ takes care of non-uniform load distribution on the tooth contact surface due to misalignment resulting from the rigidity of and clearances in gear supporting members (like bearings, shafts, and housing), manufacturing accuracy, tooth width and spacing, and geometric characteristics of the gear tooth. The design lateral rigidity of worm gear shafts is about the same as that of bevel gear drives [1]. In the case of wormsets, there is only one configuration possible: straddled worm and straddled gear, with the gear symmetrically placed on the shaft. This configuration makes for a minimum variation of stress over the face of the gear. The mesh overload factor for bevel gears is estimated from Eq. (B5a) [21]. In the absence of experimental data, it is suggested that the mesh overload factor for wormsets may be estimated as in Eq. (B5b).

$$K_m = 1.0 + 5.6b^2 \times 10^{-6} \quad (B5a)$$

$$K_m \approx 1.05 + 5.6b^2 \times 10^{-6} \quad (B5b)$$

A 5% allowance is added in the expression of Eq. (B5b) to that of straddled mounted bevel pinion and

straddled mounted bevel gear (Eq. (B5a)) to be on the conservative side.

**B4 Rim Backup Overload Factor, $K_r$**

The Lewis bending stress formula assumes a gear tooth attached to the perfectly rigid base support. This is true only if the gear rim is sufficiently rigid or thick enough. Gear tooth base support rigidity is assessed by the rim backup ratio ($\lambda_r$) which is defined as the rim thickness divided by the whole depth of gear tooth. AGMA experimental data suggest that when the rim backup ratio is equal to or greater than 1.2, the rim rigidity factor is unity, otherwise it is above unity. The minimum backup ratio for worm gear teeth is 1.25 to 1.5 [7]. Based on this recommendation, then $\lambda_r \geq 1.2$ and $K_r = 1$ for worm gears and may be dropped from Eq. (A1).

**B5 Profile-Shifted Load factor, $K_p$**

The standard tooth profile of involute gears defined by the pressure angle is accommodated in the modified Hertz contact stress expression by the contact form factor, see Eq. (18b). It is increasingly common to employ addendum modified gears in power drives [2]. The modification can lengthen or shorten the addendum portion of the tooth and the working pressure angle for such profile modified gearsets may be different from the standard value, depending on the modification factor. The influence of addendum modification on contact stress is represented by the parameter $K_p$ that is obtained as [35, 36]:

$$K_p = \frac{\tan \phi_n}{\tan \phi_{wn}} \qquad (B6)$$

In rack gears, a positive profile-shifting is applied to the gear only, resulting in an unchanged pressure angle from the standard value, so that $K_p = 1$, and maybe dropped from Eq. (B1).

**B6 Mesh Frictional Load factor, $K_f$**

Gear mesh friction is complicated with contributions from sliding and rolling. In worm drives, sliding in the mesh is predominant and sliding friction is more significant in power loss than rolling friction. Due to the complexities of worm drives, it seems reasonable to consider mesh frictional influence from both gear mesh (worm gear) and thread (power screw) perspectives. Hence, the frictional load factor for worm drives will be assumed to consist of mesh and thread frictional load components.

Gear mesh is independent of gear geometry and comes from two surfaces sliding over one another. The gear mesh frictional load factor for cylindrical gears is estimated as [41]:

$$K_{mf} = 1 + \vartheta_m \qquad (B7)$$

The power screw or thread frictional load component arises mainly from the thread-like geometry of a power screw. This may be deduced from the normal load on gear as its mates with a power screw. The normal contact force on the gear at the pitch radius

is given by Eq. (B8a) [10]. Eq. (B8a) is transformed into Eq. (B8b) and the thread frictional load factor for wormsets is given by Eq. (B9).

$$F_{c2} = \frac{F_{t2}}{\cos \phi_n \cos \psi - \vartheta_m \sin \psi} \qquad (B8a)$$

Then:

$$F_{c2} = \frac{K_{tf} F_{t2}}{\cos \phi_n \cos \psi} \qquad (B8b)$$

where:

$$K_{tf} = \left[ 1 - \frac{\vartheta_m \tan \psi}{\cos \phi_n} \right]^{-1} \qquad (B9)$$

The effective frictional load factor in the mesh is assumed to be the product of Eq. (B7) and Eq. (B9) which is given by Eq. (B10).

$$K_f = K_{mf} K_{tf} = (1 + \vartheta_m) \left[ 1 - \frac{\vartheta_m \tan \psi}{\cos \phi_n} \right]^{-1} \qquad (B10)$$

**B7 Worm Thread Profile Load Factor, $K_w$**

As mentioned before, different types of profiles may be used for the worm thread and the common thread profiles are designated as ZA, ZN, ZK, and ZI. A special worm with a concave profile in the axial section is the CAVEX. Maitra [2] provides data (Table B1) that indicates the bending strength of the above-mentioned worm profile types.

**Table B1 Load Capability of Steel Worm Profiles, [2, p. 4.28, Table 4.5]**

| Gear Material | Thread Profile Load Capability (MPa) | | |
|---|---|---|---|
| | ZA/ZN | K/ZI | CAVEX |
| Tin Bronze * | 23.5 | 29.4 | 39.2 |
| Al-Si alloy | 11.2 | 14 | 18.6 |
| Al-Zn alloy | 7.5 | 9.3 | 12.5 |
| Cast iron | 11.8 | 14.7 | 19.6 |
| *Centrifugal casting | | | |

**Table B2: Worm Profile Load Factor ($K_w$)**

| Gear material | Worm Thread Profile Type | | |
|---|---|---|---|
| | ZA/ZN | K/ZI | CAVEX |
| Tin Bronze | 1 | 1.25 | 1.67 |
| Al-Si alloy | 1 | 1.24 | 1.65 |
| Al-Zn alloy | 1 | 1.24 | 1.67 |
| Cast iron | 1 | 1.25 | 1.66 |
| Average value | 1 | 1.245 | 1.663 |
| Worm profile load factor ($K_w$) | 1 | 0.80 | 0.60 |

Table B2 is the normalized form of Table B1 in which the strength for the ZA & ZN design was used to divide those of the other types. Because ZA & ZN designs are the most popular thread profiles, they are used as reference profiles for normalization. It is interesting to see that the normalized values are consistent for the profiles, irrespective of gear material type in columns 3 and 4 in Table B2. It is expected that company and national design standards and as well as

manufacturing practices may influence absolute bending strength values, but the normalized ratios are expected to be reasonably constant.

From the elementary strength of materials, bending stress is directly proportional to load; therefore, Table B2 may be interpreted as relative load capability. From the average value row in Table B2, it means that on average, **1.245 N** load on ZK & ZI profiles will produce the same bending stress that **1 N** load will induce in ZA & ZN profiles. Similarly, **1.663 N** load on CAVEX profile will produce the same bending stress that **1** N will induce in ZA & ZN profiles. Therefore, the reciprocals of these average values give the relative load capability of these steel worm thread profile designs. The last row of Table B2 indicates the profile load factors for the worm thread profile types.

When $K_p = 1$ and $K_r = 1$, then Eq. (B1) reduces to:

$$K_s = K_a K_v K_m K_f K_w \qquad (B11)$$

**Appendix C: Pitting Strength of Bronze Worm Gears**

The theoretical contact strength of materials in static or rolling contact was derived in [39] and is presented in Eq. (C1a). For bronze materials, $\upsilon = 0.35$, [16, 20] and Eq. (C1b) gives theoretical contact strength.

$$S_c^* = \frac{(1.282 + 1.15\upsilon)S_{yc}}{\sqrt{1 - 2\upsilon(1 - \upsilon)}} \qquad S_c^* = 2.2818\,S_{yc} \quad (C1)$$

When work-hardening is considered, the nominal contact strength of materials for wormsets may be expressed as in Eq. (C2):

$$S_c^{/} = k_p k_w S_c^* \qquad (C2)$$

The service pitting strength is estimated with Eq. (3a) while the effective pitting strength adjustment factor is obtained from Eq. (C3b).

$$S_c = S_c^{/} Z_c \qquad Z_c = Z_n Z_r Z_x Z_v \qquad (C3)$$

During run-in, the softer bronze gear teeth surfaces are work-hardened by the harder worm thread surfaces. Japan Industrial Standards (JIS) [27] provides an empirical expression for a work-hardening factor for steel gear materials in pitting resistance and is approximately obtained as:

$$k_w = 1.2 - \frac{H_2 - 140}{1800} \quad \text{for } 140 \le H_2 \le 500 \qquad (C4)$$

Ishibashi et al. [37] found that a bronze material showed better hardenability than steel material in an experimental study on pitting failure. Of particular interest in that study is the fact that the hardness profile, or the variation of hardness against depth, from the surface for the steel and bronze gears after work–hardening has a similar pattern. Therefore, it will be conservative to estimate bronze material work hardening factor using the formula (Eq. (C4)) for steel material.

The hardness of cast bronze is generally in the range of 60 to 150 HVN and that of heat-treated bronze materials is in the range of 180 to 250 HVN. The hardness of cast brass is in the range of 45 to 100 HVN [2, 6]. Therefore, a conservative value for the work-hardening factor for cast copper alloys from Eq. (C4) is:

$$k_w = 1.2 - \frac{250 - 140}{1800} = 1.14$$

The value of $k_p = 1.155$ [39], and with $k_w = 1.14$, then from Eq. (C2):

$$S_c^{/} = 1.155 \times 1.14 \times 2.281 S_{yc} = 3.0 S_{yc}$$

When the result above, is substituted in Eq. (C3a), then:

$$S_c = 3.0 S_{yc} Z_c \qquad (C5)$$

Note that for ductile materials the compressive yield strength is approximately equal to the tensile yield strength.

The velocity factor from [16] is given in Eq. (C6a). However, results in KISSsoft [20] and MITCalc [40] for tin-phosphor bronze, indicated somewhat less conservative values compared with calculated results from Eq. (C6a) that were derived from data for all bronze types. The new information has led to a revision of Eq. (C6a) to obtain (C6b) for tin-phosphor bronzes.

$$Z_v = e^{-0.219 V_s^{1/3}} \qquad Z_v = e^{-0.193 V_s^{1/3}} \qquad (C6)$$

Eq. (C6a) is still suggested for tin-less bronzes, while Eq. (C6b) is being suggested for tin bronzes.

The parameter $Z_c$ may be obtained from Eq. (C3b). A reliability factor of $Z_r = 1.0$ is usually associated with a reliability of 99% [11], which is assumed in this study. Also, it is assumed that the durability factor $Z_n = 1.0$ and size factor $Z_x = 1.0$ in the current analysis. Therefore, Eq. (C3b) reduces to Eq. (C7).

$$Z_c = Z_v = e^{-0.193 V_s^{1/3}} \qquad (C7)$$

Bronze is the basic material for worm gears which are often manufactured as composite for economic reasons where a bronze ring gear on a rim is put on a steel or cast-iron wheel.

High in (Sn > 5%) bronzes, especially with Sn content of 10-12%, are best for high loads and high sliding speeds. Their application can only be justified in highly loaded transmissions and with a sliding speed exceeding 10 m/s. Bronze with lower Sn content (5-6%) can be used for speeds of 4 -10 m/s [40].

No specific type of bronze material is named for the worm gears in Examples 1 and 2. Now, a popular material used for most worm gears is C90700 (SAE 65) phosphor bronze [11, p. 567] which will be chosen for these Examples. The worm gears will be assumed to be made by casting using C90700 material, which has a yield strength of 152 MPa and tensile strength of 303 MPa [38]. The material for Examples 3 and 4 has a yield strength of 180 MPa and tensile strength of 300 MPa.

Using Eqs. (C5) and (C7), Table C1 summarizes the pitting velocity factor, nominal pitting strength, and service pitting strength for Examples 1 to 4.

**Table C1: Service Pitting Strength Examples**

| Example | $V_s$ (m/s) | $Z_v$ | $S_{yt}$ (MPa) | S'c (MPa) | $S_c$ (MPa) |
|---------|-------------|-------|----------------|-----------|-------------|
| 1 | 4.10 | 0.734 | 150 | 450 | 330 |
| 2 | 6.30 | 0.700 | 150 | 450 | 315 |
| 3 | 5.80 | 0.707 | 180 | 540 | 382 |
| 4 | 2.90 | 0.759 | 180 | 540 | 410 |

The nominal pitting strength estimate, in Table C1 for Example 3 is 382 MPa, which becomes 371 MPa after the same size adjustment factor of 0.97 in [40] is applied. The previous service pitting strength for Example 3 with size adjustment is 361 MPa [40]. The service pitting strength deviation of the current estimate from the previous value of [40] is 2.77% for Example 3. The previous service pitting strength estimate is 443 MPa for Example 4 in [20]. The corresponding value in the current study is 410 MPa for this example. The variance between previous and current service pitting strength for Example 4 is -7.45%. The nominal pitting strength for Examples 3 and 4 material is 520 MPa in [20, 40] and 540 MPa in this study. The variance of the current value from the previous one is 3.85%. It may then be concluded from the variances above that the scheme used for estimating the nominal and service pitting strengths of bronze materials in this section appears acceptable.

## МОДЕЛ КАПАЦИТЕТА КОНТАКТНОГ НАПОНА У ЦИЛИНДРИЧНИМ ПУЖНИМ ПРЕНОСНИЦИМА

### Е. Осакуе, Л. Анетор

Израз за капацитет контактног напона је изведен за цилиндричне пужне преноснике посматрањем пужа као спиралне летве која се спаја са завојним зупчаником. Концепт еквивалентног цилиндричног зупчаника за спирални зупчаник дефинисан тре–нутним радијусом закривљености у виртуелној равни спиралног зупчаника се користи у форму–лацији модела капацитета контактног напрезања. Сви основни пројектни параметри пужа и зупча–ника уграђени су у израз који експлицитно показује утицај основног и називног углова спирале на контактно напрезање. Узимајући у обзир геомет–рију пужа и зупчаника у захватању, активна предња ширина зупчаника и активна дужина навоја пужа се дефинишу и користе за процену поделе оптерећења међу зупцима зупчаника. Ово омогућава да интеракција кретања и сила у мрежама пужа буде обухваћена полу-емпиријским фактором, што је аспект који раније није разматран. Нови модел такође обухвата вишеструке навојне пужеве који до сада нису испитани. Израз фактора радног опте–рећења за цилиндричне зупчанике је модификован за пужне преноснике како би се узели у обзир различити дизајни профила пужних навоја и трење мреже.

Четири илустративна примера прорачуна контак–тног напрезања су изведена коришћењем новог модела капацитета контактног напона за дизајн пужних преносника из различитих референци. Процене контактног напона из новог модела су упоређене са претходним вредностима. Процењене процентуалне варијације између вредности прет–ходног и новог модела су у опсегу од -4,5% до 0,3%. Ове разлике указују на одлично до веома повољно поређење које би требало да улива извесно поверење у коришћење новог модела за задатке прелиминарног пројектовања цилинд-ричних пужних преносника.